RSC Advances

REVIEW

View Article Online
View Journal | View Issue

Cite this: *RSC Adv.*, 2023, **13**, 23991

A mini review on recent progress of steam reforming of ethanol

Xiaoqian Feng, * Yilin Zhao, Yonghua Zhao, Huan Wang, Huimin Liu * and Qijian Zhang *

Received 26th April 2023
Accepted 30th July 2023

DOI: 10.1039/d3ra02769d

rsc.li/rsc-advances

H_2 is one of the promising renewable energy sources, but its production and transportation remain challenging. Distributed H_2 production using liquid H_2 carriers is one of the ideal ways of H_2 utilization. Among common H_2 carriers, ethanol is promising as it has high H_2 content and can be derived from renewable bio-energy sources such as sucrose, starch compounds, and cellulosic biomass. To generate H_2 from ethanol, steam reforming of ethanol (SRE) is the most common way, while appropriate catalysts, usually supported metal catalysts, are indispensable. However, the SRE process is quite complicated and always accompanied by various undesirable by-products, causing low H_2 yield. Moreover, the catalysts for SRE are easy to deactivate due to sintering and carbon deposition under high reaction temperatures. In recent years, lots of efforts have been made to reveal SRE mechanisms and synthesize catalysts with high H_2 yield and excellent stability. Both active metals and supports play an important role in the reaction. This mini-review summarizes the recent progress of SRE catalysts from the view of the impacts of active metals and supports and draws an outlook for future research directions.

Introduction

With the continuous progress of industrialization, the energy problem has become an important bottleneck hindering the development of human society and environmental protection. Over-exploitation and utilization of unrenewable fossil fuels have generated huge CO_2 emissions, resulting in global warming and extreme weathers.[1] To achieve sustainable development, carbon neutrality becomes a common goal for the whole human race.[2,3] Developing sustainable energy sources to replace fossil fuels is one of the most important paths.[4,5]

Hydrogen has a high calorific value, while its combustion process only produces water. Therefore, it is one of the cleanest energy sources and is also a preferred energy carrier.[6–8] However, on the one hand, currently, the World's hydrogen production (~96%) still relies on unrenewable fossil sources, such as coal gasification and steam reforming of natural gas.[9–12] In order to reduce CO_2 emissions, renewable energy sources should be used as raw materials for hydrogen production as much as possible.[13] On the other hand, due to the low density and explosive nature of hydrogen itself, the storage conditions and transportation environments of H_2 are relatively harsh. Distributed hydrogen production using liquid hydrogen carriers is a promising way to overcome such shortcomings, as liquid is much more convenient for storage and transportation.[14]

Bioenergy is a kind of renewable energy source and its rational utilization can reduce pollution caused by the incineration of agricultural wastes. Several promising liquid H_2 carriers, including bio-oil,[15] bioethanol,[16] and biobutanol[17] can be obtained from bioenergy. Bioenergy-generated H_2 carriers can achieve the ideal state of zero net CO_2 emissions because CO_2 produced during hydrogen production from bioenergy can be recycled to bioenergy in plants through the photosynthesis process.[18,19] Among these carriers, bio-ethanol can be fermented from various easily available raw materials containing sucrose, starch compounds, and cellulosic biomass.[20,21] It also has the advantages of high hydrogen content, non-toxicity, easy storage, and processing. Therefore, producing hydrogen from ethanol reforming process has gained widespread attention.

The ethanol reforming process can be achieved by different oxidants, including O_2, H_2O, and CO_2 and can be accordingly divided into the following ways: steam reforming of ethanol (SRE), partial oxidation of ethanol (POE), dry (carbon dioxide) reforming of ethanol (DRE), and autothermal reforming of ethanol (ATRE).[22,23] The main chemical reaction equations are listed as eqn (1)–(5), while the concise pros and cons of each reaction are shown in Fig. 1.

(1) Steam reforming of ethanol

$$CH_3CH_2OH + 3H_2O \rightarrow 6H_2 + 2CO_2,\ \Delta H_{298}{}^{\theta} = 174.2\ \text{kJ mol}^{-1} \quad (1)$$

$$CH_3CH_2OH + H_2O \rightarrow 4H_2 + 2CO,\ \Delta H_{298}{}^{\theta} = 256.8\ \text{kJ mol}^{-1} \quad (2)$$

School of Chemical and Environmental Engineering, Liaoning University of Technology, Jinzhou, 121001, China. E-mail: fengxq@lnut.edu.cn; liuhuimin08@tsinghua.org.cn; zhangqijian@tsinghua.org.cn

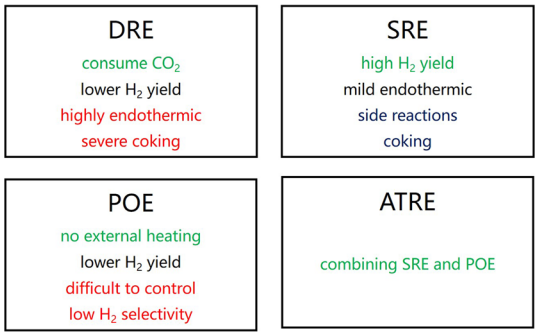

Fig. 1 Pros and cons of different paths of ethanol reforming.

(2) Partial oxidation of ethanol

$$CH_3CH_2OH + 3/2O_2 \rightarrow 3H_2 + 2CO_2,\ \Delta H_{298}{}^{\theta} = -552.0\ \text{kJ mol}^{-1} \quad (3)$$

(3) Dry reforming of ethanol

$$CH_3CH_2OH + CO_2 \rightarrow 3H_2 + 3CO,\ \Delta H_{298}{}^{\theta} = 296.7\ \text{kJ mol}^{-1} \quad (4)$$

(4) Autothermal reforming of ethanol

$$CH_3CH_2OH + H_2O + O_2 \rightarrow 4H_2 + 2CO_2,\ \Delta H_{298}{}^{\theta} = -311.3\ \text{kJ mol}^{-1} \quad (5)$$

POE process (eqn (3)) is highly exothermic and can take place without an external heating source.[24] But as oxygen is highly oxidative, the reaction is very difficult to control due to its high reaction rate.[25] As a result, ethanol is easy to be overoxidized to form H_2O and CO_2, resulting in quite low H_2 selectivity. The large heating release also leads to the formation of hotspots and the deactivation of catalysts. DRE process (eqn (4)) is a promising pathway as it can consume the greenhouse gas CO_2 to generate H_2.[26] However, due to the highly endothermic nature of the reaction and weak oxidation ability of carbon dioxide, the catalysts for this process suffer severe coking and sintering and thus deactivate quickly. Meanwhile, the theoretical H_2 yield for both POE and DRE is 3 mol H_2 per mol ethanol, which is unsatisfactory. Comparing with POE and DRE processes, SRE (eqn (1) and (2)) is more promising for pragmatic application at present. As early as 1996, Freni *et al.* verified the success of using hydrogen production by SRE in fused carbonate fuel cells.[27] Since then, SRE has attracted extensive attention from researchers. As the oxidizability of water is moderate, the SRE process is easy to control. Though it is endothermic, the required temperature is not very high (usually between 400 °C and 650 °C). It also has the highest H_2 yield that can reach up to 6 mol H_2 per mol C_2H_5OH (eqn (1)). However, the reaction temperature still leads to unneglectable sintering while various side reactions generate lots of undesirable by-products, including carbon deposition. As a result, the application of SRE is still limited by catalyst deactivation and low selectivity. Such problems have attracted the interest of many researchers in recent years.[28–30] Works are mainly concentrated on modifying the reaction process and designing appropriate catalysts.

Combining SRE and POE to form ATRE (eqn (5)) is an effective way to prolong the process, as the heat released from POE can be used for the steam reforming reaction. The reaction temperature can be remarkably reduced to avoid sintering and the strongly oxidative O_2 can help eliminate coking. However, the details and recent developments of the ATRE process have been discussed in several comprehensive reviews and are not the key points of this paper.[22,31–33] This review will focus on recent developments in the design of catalysts based on SRE mechanisms.

Mechanism study of SRE

From the perspective of thermodynamics, high temperature and low pressure benefit higher ethanol conversion as SRE is an endothermic reaction with increasing volume. Meanwhile, comparing eqn (1) and (2), it is obvious that a high water/ethanol ratio leads to high ethanol conversion and H_2 yield. Previous studies on the thermodynamics of the SRE process verified that SRE becomes dominant with excessive H_2O at >700 K and atmospheric pressure.[34,35] However, from the perspective of industrialization, higher reaction temperature means more energy consumption, higher requirements for equipment, and more inclination for catalyst deactivation. A highly active catalyst with high stability is needed to reduce the reaction temperature as much as possible. On the other hand, from the perspective of kinetics, SRE is a complicated multi-step process containing a variety of main reactions and side reactions. Lots of undesirable by-products may be generated at different temperatures, causing negative impacts such as catalyst deactivation, low H_2 yield, or harmful impurities for downstream applications.[22,23] Therefore, it is necessary to make clear the detailed mechanisms of SRE and design catalysts with expected selectivity.

The most commonly used SRE catalysts are supported catalysts with active metals (usually group VIII metals and Cu) supported on thermostable supports (such as CeO_2, Al_2O_3, SiO_2, ZrO_2, *etc.*).[36–43] These metals are the main active sites for C–C and C–H cracking. Supports can help achieve high dispersion of metals and can also participate in the reaction themselves, depending on the surface properties. Despite the fact that the mechanism of SRE on such catalysts has not been completely revealed, the generally accepted one is: ethanol absorbs dissociatively to form ethoxy species, which are further oxidized by active oxygen species (provided by the support or the dissociation of H_2O) to dehydrogenate and form acetate species. Then, on metal active sites, acetate species demethanate to form CH_x species, which are further oxidized by water to form H_2 and carbonate species, which decompose into CO_2.[44,45] However, as the SRE process is quite complicated, the specific reaction mechanisms vary with different catalysts and the intermediates often undergo undesirable side reactions at different conditions. Lots of researchers have carried out most possible reactions in the SRE process, shown in eqn (6)–(23) and Fig. 2:[23,46]

$$C_2H_5OH \rightarrow C_2H_4 + H_2O \quad (6)$$

$$C_2H_4 + 2H_2O \rightarrow 2CO + 4H_2 \quad (7)$$

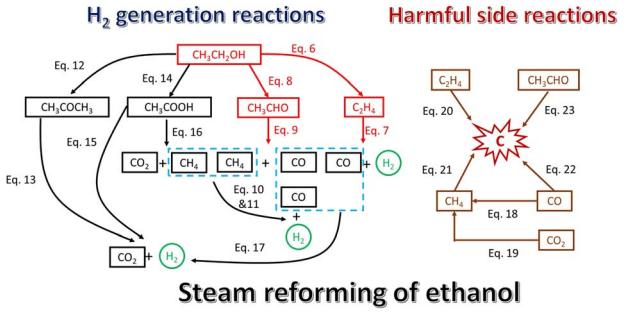

Fig. 2 Main H_2 generation reactions and harmful side reactions in SRE.

$$C_2H_5OH \rightarrow CH_3CHO + H_2 \quad (8)$$

$$CH_3CHO \rightarrow CH_4 + CO \quad (9)$$

$$CH_4 + H_2O \rightarrow CO + 3H_2 \quad (10)$$

$$CH_4 + CO_2 \rightarrow 2CO + 2H_2 \quad (11)$$

$$2C_2H_5OH \rightarrow CH_3COCH_3 + CO + 2H_2 \quad (12)$$

$$CH_3COCH_3 + 5H_2O \rightarrow 8H_2 + 3CO_2 \quad (13)$$

$$C_2H_5OH + H_2O \rightarrow CH_3COOH + 2H_2 \quad (14)$$

$$CH_3COOH + 2H_2O \rightarrow 2CO_2 + 4H_2 \quad (15)$$

$$CH_3COOH \rightarrow CO_2 + CH_4 \quad (16)$$

$$CO + H_2O \rightarrow CO_2 + H_2 \quad (17)$$

$$CO + 3H_2 \rightarrow CH_4 + H_2O \quad (18)$$

$$CO_2 + 4H_2 \rightarrow CH_4 + 2H_2O \quad (19)$$

$$C_2H_4 \rightarrow [C_2H_4]_n \rightarrow \text{coke} \quad (20)$$

$$CH_4 \rightarrow C + 2H_2 \quad (21)$$

$$2CO \rightarrow C + CO_2 \quad (22)$$

$$CH_3CHO \rightarrow \text{coke} \quad (23)$$

The occurrence of these reactions highly depends on different reaction conditions and different types of catalysts. Generally, in the presence of acid catalysts, ethanol is easy to dehydrate to generate ethylene (eqn (6)), and ethylene may also be reformed with water to generate carbon monoxide and hydrogen (eqn (7)). However, excessive generation of ethylene reduces the hydrogen yield as it contains high contents of hydrogen. Ethylene polymerization reaction (eqn (20)) leads to severe coking and catalysts' deactivation.[47] Hence, ethanol's dehydration should be avoided as far as possible. On the contrary, ethanol is prone to dehydrogenation on catalysts with alkaline active sites to generate acetaldehyde (eqn (8)), and the resulting acetaldehyde will decompose into methane and carbon monoxide (eqn (9)). The resulting methane will undergo further reforming reaction with water (eqn (10)). When the reaction temperature is high enough, the dry reforming of methane (eqn (11)) also occurs to form carbon monoxide and hydrogen. Thorough transformation of CH_4 to H_2 is anticipated to get a high H_2 yield. Besides, there exists several marginal side reactions such as ethanol ketonization (eqn (12)), acetone steam reforming (eqn (13)), and ethanol oxidation to acetic acid (eqn (14)), while acetic acid also continues to undergo reforming (eqn (15)) and decarbonization (eqn (16)). CO generated by any reactions can be transferred to CO_2 through water–gas shift reaction (eqn (17)). As CO is an important poisonous species for the catalysts in proton exchange membrane fuel cells, it is quite necessary to promote WGS process and reduce the ratio of CO in the products. The methanation reaction of carbon monoxide and carbon dioxide (eqn (18) and (19)) is undesirable as it consumes the target product H_2.

The main reason for catalyst deactivation in SRE is the formation of coke, which is generated from several side reactions, including ethylene decomposition (eqn (20)), methane decomposition (eqn (21)), CO disproportionation (eqn (22)) and acetaldehyde cyclization (eqn (23)). Coke is of two main types: encapsulated coke and filamentous coke. Encapsulated coke will block active sites and directly deactivate catalysts. Filamentous carbon usually shows no significant impact on the activity of catalysts, but large amount of that will lead to bed blockage.[36] Both ethylene and acetaldehyde are the main precursors to the formation of encapsulated coke, and methane decomposition and carbon monoxide disproportionation are responsible for the formation of filamentous coke.[48] The major pathway for the gasification of coke is the reverse reaction of CO disproportionation, which can be promoted by alkaline sites on catalysts, and water–gas reaction (WGR), which is favored by excessive water. On the other hand, the nucleation process of carbon is also an important factor for carbon deposition. It is widely accepted that the nucleation of carbon deposition is favoured on terrace sites.[49–51] Therefore, increasing the fraction of edge and corner, namely, smaller metal particle sizes, can limit the nucleation as well as the accumulation of coke.

In comprehensive consideration, an ideal SRE catalyst should possess the property that the cracking of C–C and WGS can be promoted while ethanol dehydration and other coke-forming reactions can be avoided as far as possible. It should also show a low affinity to coke and benefit carbon gasification. The surface acidity/basicity of supports provides active sites for ethanol dehydration/dehydrogenation and significantly impacts the selectivity. Generally, moderate alkaline supports or adding alkaline promoters can suppress ethanol dehydration and benefit coke gasification. High dispersion (small particle size) of loaded active metals should be ensured for higher activity and better coking resistance, while sintering at high temperatures should be suppressed.

Recent research on SRE catalysts

In recent years, researchers have developed SRE catalysts with excellent H_2 yield and stability. The development of *in situ*

techniques makes it possible to comprehend the mechanisms more precisely.

The effects of active metals

Noble metals such as Rh, Ru, and Pt exhibit excellent comprehensive performance in SRE. Liguras *et al.* compared SRE performances of supported Rh, Ru, Pt, and Pd in the temperature range of 600–850 °C.[52] It was found that Rh shows higher catalytic activity and H_2 selectivity than Ru, Pt, and Pd at low metal loading. Ru shows catalytic performance proportional to the loading of metal. When the loading is 5%, the catalytic activity and selectivity of Ru, which is much cheaper, can be comparable to the very expensive Rh. Under certain conditions, the conversion rate of ethanol on 5% Ru/Al_2O_3 can reach 100%, and the selectivity of hydrogen is as high as 95% while the only by-product is methane. The stability of Ru/Al_2O_3 is also acceptable for a downstream fuel cell. Bilal *et al.* compared the SRE performance of Rh and Pt supported on Al_2O_3.[53] At 773 K, Rh/Al_2O_3 shows higher activity and the main by-product is liquid products such as acetaldehyde and acetone, while ethylene is the main by-product on Pt/Al_2O_3. However, at 873 K, Pt/Al_2O_3 is more active and shows higher H_2 selectivity than Rh/Al_2O_3. Both Pt and Rh catalysts forms graphitic coke, the disorder of which generally increases with increasing reaction temperature. de Lima *et al.* evaluated the SRE performance of $ZrCeO_2$ with or without Pt loading.[54] $Pt/ZrCeO_2$ shows high conversion and H_2 selectivity as Pt facilitates the decomposition of acetate species. However, the accumulating coke blocks the boundary between Pt and $ZrCeO_2$ support, hindering the demethanation of acetate species located on $CeZrO_2$ support, leading to severe deactivation.

Generally, noble metals supported on appropriate supports have pretty good comprehensive performance in SRE. However, the high price makes them unsuitable for large-scale use in industrial applications. Therefore, in recent years, noble metal-based catalysts are usually used as model catalysts for exploring the role of support or SRE mechanisms.[55–58] In order to explore more applicable catalysts, researchers mainly focus on non-noble metal catalysts due to their low price and high catalytic activity.[59,60] The most studied non-noble metals include Ni, Co, and Cu. Ni-based catalysts have excellent ability for C–C cleavage but are easy to deactivate due to sintering and carbon deposition.[6,61] Co shows good activity and can suppress the generation of CH_4.[28] Cu catalyst is beneficial for ethanol dehydrogenation while Cu active sites can promote WGS, so as to improve hydrogen selectivity. However, Cu has a low ability for C–C breaking and is usually used as a second metal.[47] Rossetti *et al.* investigated the SRE performance of Ni, Co, and Cu supported on SiO_2 prepared by incipient wetness impregnation.[62] Ni shows excellent activity, H_2 selectivity, and limited by-products whereas carbon accumulation was observed. Co also shows high ethanol conversion while H_2 selectivity is only high at higher temperatures (500 °C). However, the activity of Co for acetaldehyde reforming is quite low, especially at lower temperatures (400 °C), leading to a large amount of acetaldehyde. As for Cu, ethanol conversion is low while acetaldehyde is dominant. Di Michele *et al.* loaded Ni on $MgAl_2O_4$ and investigated the effect of Ni content on SRE activity.[63] With the increase in Ni content, both ethanol conversion and H_2 selectivity increase, and the catalyst exhibits good stability at 625 °C and atmospheric pressure. *In situ* diffuse reflectance infrared spectroscopy characterization showed that most ethanol is converted to acetaldehyde through oxidative dehydrogenation rather than decomposition reactions. A small amount of ethylene produced can undergo reforming and conversion under the catalysis of Ni, resulting in less carbon deposition. The main type of carbon deposition is amorphous carbon, which is easy to regenerate through oxidation. Greluk *et al.* studied the effect of Co loading on the SRE activity of Co/CeO_2 catalysts.[36] A higher Co loading amount (29 wt%) enhances the interaction between Co and CeO_2 while not excessively increasing the size of Co particles, thereby exhibiting the best ethanol conversion and H_2 selectivity at 500 °C and atmospheric pressure. However, the catalyst also experiences severe carbon deposition during long-term reactions, resulting in a decrease in reaction activity.

To overcome the shortage of each single non-noble metal, alloys are usually introduced to modify the surface characteristics to adjust the reaction mechanism and achieve high H_2 selectivity and coke resistance.[64,65] The addition of a small amount of noble metal can improve the performance.[66,67] For example, Campos *et al.* added 1% Rh into 10% Ni/15% La_2O_3–10% CeO_2–Al_2O_3 catalyst for SRE.[68] The addition of Rh favors C–C bond breaking, the hydrogenation of CH_x species, and the desorption of CO. Compared with the catalyst without Rh addition, the carbon deposition in 1% Rh–10% Ni catalyst reduces by 560 times. The small amount of carbon can be removed easily by regeneration in air, and the activity of the catalyst can be fully recovered. Sanchez-Sanchez *et al.* reported $NiPt/Al_2O_3$ benefits the gasification of methyl groups formed in the decomposition of acetate species and achieves higher activity and stability than Ni/Al_2O_3.[69]

Appropriate non-noble metal addition can also modify the surface properties and promote SRE performance. Michał *et al.* prepared Cu/ZrO_2 catalysts doped with Mn, Ni, and Ga by co-precipitation method with ZrO_2 as the support and evaluated their SRE performance at 350 °C.[70] Without a second metal, acetaldehyde is generated on Cu/ZrO_2, and acetaldehyde further reacts to produce C_1 by-products (CO and CH_4) and carbon deposition, leading to deactivation of the catalyst. Compared with the unmodified Cu/ZrO_2 catalyst, the addition of dopants not only effectively inhibits coking but also increases the hydrogen yield and ethanol conversion rate. Among all the modified catalysts, the highest hydrogen yield is achieved on $Cu–Ni/ZrO_2$ (52%). The addition of Ni promotes the breaking of the C–C bond, increases the selectivity of C_1 gases (CO, CO_2, and CH_4), and reduces the formation of acetaldehyde. Lorenzut *et al.* prepared a $Cu/ZnO/Al_2O_3$ catalyst and found that a single metal Cu can only catalyze the dehydrogenation of ethanol due to the poor activity for C–C cleavage, resulting in a low H_2 selectivity.[71] The introduction of Ni or Co can significantly improve H_2 selectivity. The formation of Ni–Cu alloy allows Cu to occupy active step positions, which are prone to carbon deposition, on

the surface of Ni particles, thereby significantly resisting coking. However, Co cannot form an alloy with Cu, and there is no synergistic effect between Co and Cu. Therefore, Co still exhibits the properties of a single metal Co, resulting in a large amount of carbon deposition. Han *et al.* prepared a series of mesoporous Cu–Ni–Al_2O_3–ZrO_2 catalysts with different copper contents for SRE.[72] It is found that with the increasing copper content, the catalytic performance of the catalyst first increases and then decreases. A small amount of Cu can promote ethanol dehydrogenation reaction, but excessive Cu will occupy Ni active sites, which is unfavorable for the cleavage of C–C bonds. Therefore, the highest H_2 yield can only be achieved at moderate Cu content. Chen *et al.* also reported that Ni_9Cu_1/YSZ catalyst shows good H_2 yield and less coke formation in SRE, while an overdose of Cu (Ni_8Cu_2) leads to low activity.[60] Wang *et al.* prepared $LaFe_{1-x}Co_xO_3$ and further reduced it to obtain a Ni–Co alloy catalyst, which exhibits excellent activity and stability in SRE at 650 °C, atmospheric pressure and quite high WHSV = 240 000 ml $g_{cat}^{-1}\cdot h^{-1}$.[73] The ratio of Ni to Co has a direct impact on the activity of the catalyst. Increasing Ni content can improve the conversion of ethanol and H_2 selectivity. The formation of Ni–Co alloy can also improve the interaction between the metal and support and enhance the sintering resistance. Braga *et al.* studied in detail the SRE mechanism of Ni–Co alloy supported on $MgAl_2O_4$.[74] *In situ* XANES analysis revealed that at lower reaction temperatures, moderately loaded Ni–Co could form smaller alloy particles. More CoO exists on its surface due to its high oxygen affinity. CoO mainly catalyzes the dehydrogenation of ethanol but is not active for C–C breaking, so the main product at a low temperature (350 °C) is acetaldehyde. As the temperature of the reaction increases to 450–550 °C, part of CoO is *in situ* reduced to expose the active sites of the Ni–Co alloy, which is active for the cracking of the C–C bond. Meanwhile, the remaining part of CoO on the surface can inhibit the formation of surface carbon. Such transformation is shown in Fig. 3.

Wu *et al.* studied the role of Ni–Fe alloy in Ni–Fe/$MgAl_2O_4$ catalyst for SRE.[75] Within Ni–Fe alloy, the transfer of electrons from Fe to Ni weakens CO adsorption and reduces CO and CO_2 methanation. At high steam-to-carbon ratio, part of Fe can be oxidized by water to form γ-Fe_2O_3 species, which can promote the transformation of ethoxy to acetate groups to avoid methane formation. The oxidation ability of γ-Fe_2O_3 species also benefits coking elimination. The $Ni_{10}Fe_{10}/MgAl_2O_4$ catalyst thus shows a very high H_2 yield (4.6 mol per mol ethanol) and good stability at 400 °C during a 30 h test.

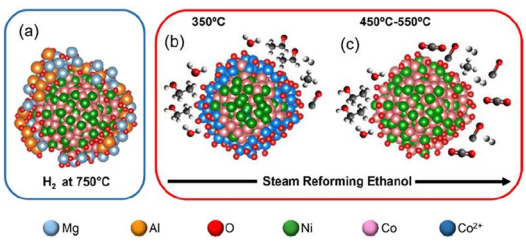

Fig. 3 The schematic of the transformation of the surface of NiCo alloy. Reprinted with permission from ref. 70. Copyright 2021, American Chemical Society.

A summary table of recent representative progress on SRE catalysts with different active metals is shown in Table 1. Generally, non-noble metal-based catalysts are indeed practicable catalysts for SRE in the future due to their low cost. As Ni, Co, and Cu play different roles in ethanol dehydrogenation and C–C breaking, it is important to design alloys with appropriate components to achieve high H_2 yield and stability. The surface properties of alloys are very important for the reaction mechanisms and directly impact the comprehensive performance of the catalysts. Further research studies are still needed for a deep understanding of the relationship between the surface properties of alloys and reaction mechanisms.

Apart from active metals, the supports in SRE catalysts also play a significantly important role. The specific surface area of the supports directly affects SRE performance, while well-designed porous structures can confine metal nanoparticles to resist sintering. Silva *et al.* explored the catalytic performance in SRE at 500 °C of Rh loaded on CeO_2 with low (~14 $m^2\ g^{-1}$) or high (~275 $m^2\ g^{-1}$) specific surface area.[44] The H_2 selectivity of pure CeO_2, regardless of specific surface area, is low due to its poor ability to break C–C bonds. After loading Rh on CeO_2, the ethanol conversion rates as well as H_2 selectivities of the two Rh/CeO_2 catalysts are significantly improved. Raman spectrum analysis showed that carbon deposition can be found on the surface of spent Rh/CeO_2 with a low specific surface area. Whereas Rh/CeO_2 with a high specific surface area exhibits good coke resistance as a large amount of active oxygen species on the surface of CeO_2 helps the elimination of coke. Various kinds of mesoporous SiO_2 have been used as supports due to their high surface area and confinement effect.[76–78] Elharati *et al.* compared SBA-15 and commercial SiO_2 as the support for Ni–Mo bimetallic SRE catalyst at 600 °C and atmospheric pressure.[79] The ordered mesoporous structure of SBA-15 as well as the high specific surface area ensures the high dispersion of NiMo, and the mesopores restrain carbon formation. Therefore, NiMo/SBA-15 shows much better activity and superior coking resistance than NiMo/SiO_2. Parlett *et al.* prepared a multi-level porous SBA-15 carrier with both macropores and mesopores, and then loaded Ni nanoparticles.[80] The extremely high specific surface area and a large number of pores ensure a high dispersion of Ni. When the loading amount of Ni reaches 10 wt%, it can still maintain an ultra-fine particle size of ~3 nm, providing many active sites, which result in high activity. On the other hand, the bimodal porous structure greatly benefits the diffusion of reactive gases. The very short residence time of the reactants and products decreases the coke formation. Costa *et al.* reported SBA-15 can also help achieve high dispersion of perovskite oxide $LaNiO_3$ and the derived Ni nanoparticles.[81] Compared with bulk perovskite, such catalysts show lower carbon deposition due to the smaller Ni nanoparticles.

Wang *et al.* designed a novel hierarchical core–shell beta zeolite with a petal-like shell layer containing well-dispersed Ni nanoparticles, as shown in Fig. 4.[82] Such structure helps realize the immobilization and high dispersion of the Ni at quite a high loading (~22 wt%). The catalyst shows high ethanol conversion

Table 1 Recent representative progress on SRE catalysts with different active metals

Catalyst	Preparation method	Reactor	Reaction conditions	Performance	Literature
5% Ru/Al_2O_3	Impregnation	Continuous flow microreactor	Flow rate: 340 cm^3 min^{-1}, temperature = 800 °C, atmospheric pressure, H_2O : EtOH = 3 : 1	Ethanol conversion: 100%, H_2 selectivity: 95%, 100 h stable	52
Pt/Al_2O_3	Incipient wetness impregnation	Continuous flow high pressure microreactor	GHSV = 50 000 h^{-1}, temperature = 873 K, pressure: 20 bar, steam to ethanol ratio of 5 : 1	Ethanol conversion: 90%, H_2 selectivity: 55%, 40 wt% carbon deposition after 100 h	53
$Pt/ZrCeO_2$	Precipitation & incipient wetness impregnation	Fixed-bed reactor	Residence time = 0.02 g s ml^{-1}, temperature = 773 K, atmospheric pressure, H_2O/ethanol molar ratio = 5.0	Ethanol conversion: 70%, H_2 selectivity: 67%, carbon deposition observed after 30 h	54
Ni/SiO_2	Incipient wetness impregnation	Continuous downflow reactor	GHSV = 1750 h^{-1}, temperature = 500 °C, P = 1 atm	Ethanol conversion: 100%, H_2 productivity: 1.3 ± 0.3 mol min^{-1} kg_{cat}^{-1}, $H_2/EtOH_{in}$: 4.0 ± 0.7 mol mol^{-1}, no coking after 6 h	62
10% $Ni/MgAl_2O_4$	Ultra-sound assisted co-precipitation	Continuous downflow reactor	GHSV = 2700 h^{-1}, temperature = 625 °C, under atmospheric pressure	C_2H_5OH conversion: 100%, H_2 productivity: 1.23 ± 0.04 mol min^{-1} kg_{cat}^{-1}, 3.87 ± 0.13 mol H_{2out} per mol $C_2H_5OH_{in}$ 14.86 wt% coking after 8 h	63
$29Co/CeO_2$	Co-precipitation	Fixed-bed continuous-flow quartz reactor	GHSV = 60 000 ml g^{-1} h^{-1}, temperature = 500 °C, under atmospheric pressure, H_2O/EtOH = 12/1	Ethanol conversion rate of approximately 100%, H_2 selectivity ~ 95%, 24 h stable	36
1% Rh–10% Ni/15% La_2O_3–10% CeO_2–Al_2O_3	Impregnation	Tubular reactor	mol Ar per (mol H_2O + mol C_2H_5OH) = 0.76, GHSV = 26 000 h^{-1}, 500 °C	Ethanol conversion: 100%, H_2 selectivity: 57%, 144 h stable, no carbon after 24 h	68
$CuO/ZrO_2/NiO$	Co-precipitation	Fixed-bed flow reactor	Temperature = 350 °C, water/ethanol = 10	Ethanol conversion: 99%, H_2 yield: 52%, coking observed after 2 h	70
$Ni/Cu/ZnO/Al_2O_3$	Carbonate coprecipitation	U-shaped 4 mm ID quartz microreactor	GHSV = 120 000 ml g^{-1} h^{-1}, temperature = 600 °C, ethanol (1.0%) + H_2O (5.0%) in Ar	Hydrogen yield: about 50%, coking 0.3804 g_{carbon} g_{cat}^{-1} after 75 h	71
0.2Cu–Ni–Al_2O_3–ZrO_2	Single-step epoxide-driven sol–gel method	Continuous flow fixed-bed reactor	GHSV = 28 280 ml h^{-1} g^{-1}, temperature = 450 °C, atmospheric pressure, mol ratio of EtOH : H_2O : N_2 = 1 : 6 : 12.2	Ethanol conversion: 100%, H_2 yield: 86.6%, 1000 min stable	72
Cu_1Ni_9/YSZ	Wet impregnation	Fixed-bed quartz reactor	Flow rate = 0.8 ml h^{-1}, catalyst 50 mg, temperature = 650 °C, stability test time = 20 h, atmospheric pressure, mol ratio of water to ethanol = 3 : 1	Ethanol conversion: ~70%, H_2 yield: ~70%, coking observed after 20 h	60
Ni_{10}–$Co/LaFeO_3$	Citric acid complexation-impregnation	Fixed-bed quartz reactor	WHSV = 240 000 ml g_{cat}^{-1} h^{-1}, temperature = 650 °C, at atmospheric pressure	Ethanol conversion: 100%, H_2 selectivity: around 67%, ~60 wt% coking after 10 h	73
$Ni_{10}Fe_{10}/MgAl_2O_4$	Incipient co-impregnation	Quartz fixed-bed reactor	GHSV = 88 719 ml (g^{-1} h^{-1}), temperature = 400 °C, stability test time = 15 h, at atmospheric pressure	Ethanol conversion: more than 90%, H_2 yield: 4.6 mol per mol ethanol, 30 h stable, coking observed	75

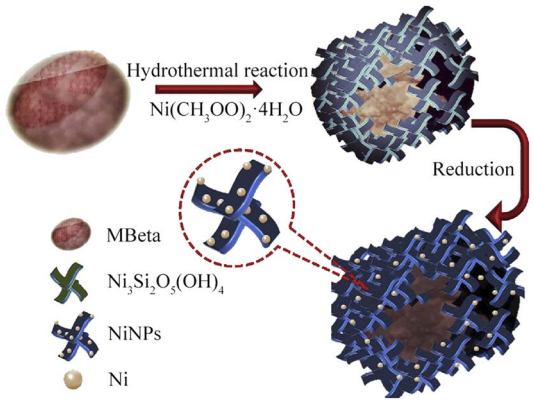

Fig. 4 Schematic of the synthesis of the hierarchical core–shell beta zeolite with a petal-like shell layer containing well dispersed Ni nanoparticles. Reprinted from ref. 82, copyright (2020), with permission from Elsevier.

(~85%) and H_2 selectivity (70%) for SRE at 550 °C, while trivial deactivation is observed after 100 h on stream at 400 °C. Marjan *et al.* applied metal–organic framework (MOFs) as support of SRE catalysts.[83] Ni nanoparticles were loaded on ZIF-8, which has a high surface area, good thermal stability, and high porosity. PEG was further used to modify the interfacial properties of ZIF-8 to achieve high Ni dispersion and suitable interfacial interactions. The resulting Ni/ZIF-8. PEG catalyst displays a high H_2 yield (52.6%) at quite a low temperature (450 °C).

The acidity and alkalinity of the supports have a direct and significant impact on the selectivity of SRE. In general, the acidic sites in the supports have a strong ability to catalyze ethanol dehydration, leading to excessive production of ethylene, which in turn leads to carbon deposition. On the contrary, more alkaline sites can suppress ethanol dehydration, thus suppressing carbon formation. Alkaline sites can also promote the adsorption of CO_2 and benefit the left-shifting of CO disproportionation (eqn (22)), accelerating the elimination of carbon deposition. Therefore, SRE catalysts typically use alkaline supports or add into the support alkaline promoters.[84,85] Batista *et al.* prepared Co/SiO_2, Co/Al_2O_3, and Co/MgO catalysts by impregnation method, which exhibit good catalytic activity (ethanol conversion > 90%) and hydrogen selectivity (about 70%) in SRE at 400 °C.[86] After a long-term reaction, carbon deposits appear on the surface of the catalysts, with the amount ranging as Co/Al_2O_3 > Co/MgO > Co/SiO_2. This is due to the strong acidity of Al_2O_3, which promotes the occurrence of ethanol dehydration reactions. More ethylene cracking results in more carbon deposition. Martinelli *et al.* found that Na loading in Pt/ZrO_2 catalyst can improve the demethanation of acetate species and increase CO_2 selectivity in SRE.[45] When the amount of Na is low, decarbonylation of acetate is preferred, and more CO will be generated. However, when Na loading is too high, the activity of the catalyst will decrease significantly. Pizzolitto *et al.* added La promoter to the Ni–ZrO_2 catalyst and evaluated the SRE performance at 550 °C.[87] The addition of La provides a large number of basic sites, which effectively inhibits the occurrence of ethanol dehydration, reducing the generation of carbon deposition and improving the stability of the catalyst. Compared to the precipitation method, adding La promoter through impregnation method has a more significant effect on improving alkalinity, with higher ethanol conversion and H_2 yield and better catalyst stability. Similar phenomena were observed by Boudadi *et al.* on La-doped Ni/Al_2O_3 catalyst.[88] However, on TiO_2 or clay supports, La promoter does not work well, probably due to its deficient dispersion. Shi *et al.* modified Ni/Al_2O_3 catalyst with Zr, Ce, and Mg promoters.[89] Mg and Ce addition can block medium and strong acid sites, which are responsible for the formation of C_2H_4. Ni/Mg–Al_2O_3 shows good coking resistance and stability during a 30 h test at 500 °C.

The interaction between metal and support also has an important impact on the comprehensive performance of the catalyst.[90] Strong metal–support interaction (MSI) can help "anchor" metal nanoparticles on supports by the formation of strong chemical bonds.[91] As a result, the sintering resistance of the metal particles enhances a lot and helps achieve higher dispersion, which leads to high activity and stability. The rational design and appropriate synthesis methods are very important for the enhancement of MSI. Liguras *et al.* loaded Ru on different oxide supports and evaluated their SRE performances.[52] Though acidic Al_2O_3 benefits undesirable ethylene formation, the Ru dispersion on Al_2O_3 is much higher than that on MgO and TiO_2 owing to the stronger interaction between Ru and Al_2O_3, leading to much better reforming activity. Therefore, Ru/Al_2O_3 shows the best ethanol conversion and H_2 selectivity. Meng *et al.* prepared RhNiTi-layered double hydroxide precursor, and the derived $0.5RhNi/TiO_2$ catalyst possesses strong MSI.[92] The Rh–$Ni^{\delta-}$–O_v–Ti^{3+} interface facilitates the formation of formate intermediate and therefore promotes H_2 production. The catalyst shows a very high H_2 yield (12.2 L h^{-1} g_{cat}^{-1}) and excellent stability (300 h) at 400 °C. Grzybek *et al.* doped K into α-Al_2O_3 and found K can improve the Lewis acidity of the α-Al_2O_3 support and enhance the MSI between loaded Co and the support.[59] The K promoted catalyst has better dispersion of Co and improved sintering resistance while Co nanoparticles' detachment caused by carbon deposition is also curbed. As a result, both selectivity and stability of the catalyst in SRE are enhanced. Further research revealed the best K doping content is 0.3 wt%.[93] It is also reported that K promoter can effectively inhibit the occurrence of the methanation reaction, thereby reducing the formation of CH_4 and improving the yield of H_2. However, excessive K can block the pore channels of the catalyst, which can lead to a decrease in activity.[94] Wang *et al.* used attapulgite (ATP), a natural hydrated magnesium aluminosilicate mineral with unique chain layer structure, as a support for Ni-based SRE catalyst.[95] The Ni loading directly affects the Ni–O–Si/Al species formed through the interface of Ni species and ATP framework. At optimized Ni loading, 20Ni/ATP shows the strongest MSI, leading to the highest anti-sintering performance, and consequently, high H_2 yield and high stability at 600 °C. Further research showed that calcination temperature also plays an important role in the MSI of Ni/ATP catalysts.[96] Higher calcination temperature leads to

stronger MSI due to the formation of more Ni(Mg, Al)–O and $(Ni_xMg_{1-x})(OH)_4Si_2O_5$ species. The carbon deposition type differs a lot at different MSI. Aromatic species can be found in spent catalysts prepared at low calcination temperature while the carbon deposition on high-temperature calcined catalyst shows higher degrees of graphitization. Zhou *et al.* achieved strong MSI between Ni and CeO_2 through the formation of $Ni_xCe_{1-x}O_{2-y}$ solid solution.[97] In the SRE process, the strong MSI helps high Ni dispersion and perturbs the electronic properties of Ni to suppress its methanation activity. Ni embedded in ceria induces the formation of O vacancies, which facilitate the cleavage of the OH bonds in ethanol and water. The $Ni_{0.2}Ce_{0.8}O_{2-y}$ catalyst shows ~100% ethanol conversion and ~67% H_2 selectivity at 400 °C.

Supports with high oxygen exchanging ability, such as CeO_2, are promising supports or promoters for SRE as they can accelerate the oxidation elimination of coking. Such supports can also help improve MSI and further increase the overall performance. Somasree *et al.* reported that the oxygen exchanging ability of CeO_2 leads to high SRE activity and stability of Rh/CeO_2/γ-Al_2O_3 catalyst.[98] At 700–800 °C, the 2% Rh/20% CeO_2/λ-Al_2O_3 catalyst generates a high H_2 yield (~60 vol%) while the amount of CO and CH_4 is very low. Luo *et al.* studied the role of CeO_x loaded on Ni_xMg_yO matrix.[99] The highly mobile oxygen species provided by CeO_x is effective for coke removal, significantly improving the stability in SRE. Meanwhile, CeO_x benefits CO adsorption and promotes WGS to achieve higher H_2 selectivity. Wang *et al.* investigated the selective Ni locations over Ni/$CeZrO_x$–Al_2O_3 catalysts.[100] When Ni content is low, Ni interacts with $CeZrO_x$ and generates more lattice oxygen, enhancing SRE activity. However, at higher Ni content, Ni interacts with Al_2O_3 after the saturation of $CeZrO_x$ sites. Compared with Ni–$CeZrO_x$ sites, Ni–Al_2O_3 sites benefit the generation of ethylene and lead to severe coking. 10 wt% Ni is found to be proper for the formation of only Ni–$CeZrO_x$ sites. Moogi *et al.* added La_2O_3 and CeO_2 additives to the synthesis process of SBA-15 and further loaded Ni for SRE.[78] The as-prepared catalyst shows good activity and stability at 650 °C. This can be partly attributed to the high specific surface area and pore structure of the SBA-15 carrier itself. The addition of La_2O_3 is beneficial for enhancing the MSI between Ni and the support, thereby improving Ni dispersion. CeO_2 additives enhance water activation by oxygen-deficient sites and promote coking elimination.

Appropriate metal doping can further enhance the oxygen mobility of CeO_2. Xiao *et al.* prepared Pr doped Ni/CeO_2 catalyst by sol–gel method and explored the influence of Pr on the catalyst properties.[101] They found that the addition of an appropriate amount of Pr can enhance the MSI between Ni and CeO_2, thus obtaining highly dispersed Ni particles. Meanwhile, the addition of Pr increases the concentration of oxygen vacancies, which can help water activation as well as the elimination of carbon species. Compared to Ni/CeO_2, the catalyst doped with 20% Pr exhibits significantly higher ethanol conversion, H_2 yield, and stability at 600 °C and atmospheric pressure. They further studied the effects of doping elements such as La, Tb, and Zr on the performance of Ni/CeO_2 and found that these elements can play a similar role in regulating metal carrier interactions and

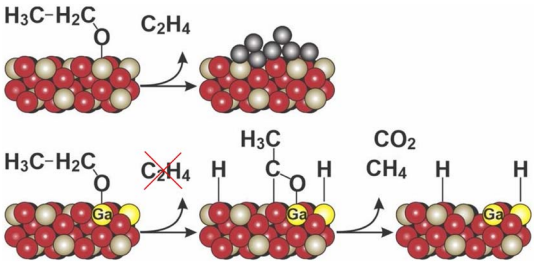

Fig. 5 Schematic of the role of Ga doping in SRE mechanisms. Reprinted from ref. 103, copyright (2020), with permission from Elsevier.

increasing oxygen vacancies as Pr. Among them, La doping has the most significant improvement in the comprehensive performance of SRE.[102] Vecchietti *et al.* studied the role of Ga doping in CeO_2 and found that Ga-doped CeO_2 shows a higher H_2/CO_2 ratio and less coking.[103] DFT calculation results showed that ethoxy species adsorb on the surface of CeO_2 in two types: standing-up and lying-down, namely, the alkyl chain more perpendicular or parallel to the surface. Standing-up adsorption converts to acetate species and further decomposes to CO_2 and CH_4. Lying-down ethoxy tends to decompose into H_2 and C_2H_4, which results in coking. The doping of Ga can facilitate the oxidation of lying-down ethoxy to acetate species instead of C_2H_4 by the formation of Ga–H species, as shown in Fig. 5.

Meanwhile, it can also generate more labile oxygen at the Ce–O–Ga interface, which assists in the decomposition of acetate species. As a result, Ga-doped CeO_2 is a promising support for high coking-resistance SRE catalysts.

The exposure facets of CeO_2 also play an important role.[104,105] Araiza *et al.* reported that CeO_2 rods with (111) facet exposure has stronger oxygen storage capacity and benefit higher Ni dispersion.[105] Compared to CeO_2 particles and cubes, such Ni–CeO_2-rod catalyst shows high H_2 yield as well as low carbon accumulation. Li *et al.* used *in situ* synchrotron radiation photoionization mass spectrometry to analyze the interaction between CeO_2 and Co.[106] It is found that Co sites on CeO_2(111) facet are in a lower oxidation state than on CeO_2(100) facet and exhibit higher C–C bond cleavage capability, resulting in better SRE performance. The conversion of ethanol can reach 100% with a H_2 selectivity of 97% at 500 °C and atmospheric pressure.

A summary table of recent representative progress on SRE catalysts with different supports is shown in Table 2. In brief, important properties of ideal supports include high surface area, appropriate alkalinity, and strong oxygen storage capability. Doped CeO_2 is one of the best choices. Well-designed nanostructures with confinement effects can achieve high metal dispersion and help resist sintering while various mesoporous structures have been explored, such as mesoporous SiO_2, MOFs, zeolites, and clays. The interaction between supports and the active metals plays a very important role in the activity and H_2 selectivity of the catalyst, as well as sintering and coking resistance. Further investigation and understanding of the metal–support interface and relevant reaction mechanisms are needed based on advanced characterization technologies.

Table 2 Recent representative progress on SRE catalysts with different supports

Catalyst	Preparation method	Reactor	Reaction conditions	Performance	Literature
Rh/CeO_2	Incipient wetness impregnation	Fixed-bed reactor	Residence time = 0.02 g s ml^{-1}, temperature = 773 K, at atmospheric pressure, H_2O/ethanol molar ratio = 3.0	Ethanol conversion: 70%, H_2 productivity: 60–70%, 28 h no coking	44
$0.5RhNi/TiO_2$	Homogeneous precipitation	Fixed-bed reactor	400 °C, 0.15 g catalyst, ethanol/water mixture (1 : 3) 0.06 ml min^{-1}, 50 ml min^{-1}, 1 atm	H_2 yield: 12.2 L h^{-1} g_{cat}^{-1}, 300 h stable	92
Co/CeO_2	Wetness impregnation	Fixed-bed U-type quartz reactor	GHSV = 34 500 ml g^{-1} h^{-1}, temperature = 500 °C, at atmospheric pressure	Ethanol conversion: 100%, H_2 selectivity: 97%, 42 h stable	105
$Ni_xMg_yO–CeO_x$	PEG-assisted precipitation	Fixed-bed reactor	700 °C, S/C = 3, GHSV = 200 000 h^{-1}, P = 1 atm	Ethanol conversion: ~90%, 4.82 mol H_2 per mol C_2H_5OH, carbon < 1 wt% after 30 h	99
$Ni/CeZrO_x–Al_2O_3$	Impregnation	Fixed-bed reactor	550 °C, H_2O/C_2H_5OH = 6, GSHV = 10 619 h^{-1}	H_2 production rate = 1863.0 μmol $g_{cat}^{-1}\cdot min^{-1}$	100
$10Ni/Pr_{0.2}CeO_2$	Citric acid-assisted sol–gel method	Stainless steel fixed-bed tubular reactor	GHSV = 44 240 ml $g_{cat}^{-1}\cdot h^{-1}$, temperature = 600 °C, at atmospheric pressure, H_2O/C_2H_5OH = 4	Ethanol conversion: 100%, H_2 yield: 7247.2 μmol min^{-1},7.2 wt% carbon after 50 h	101
2 wt% Rh/20 wt% CeO_2/λ-Al_2O_3	Standard dry impregnation	Packed-bed reactor	GHSV = 5000 h^{-1}, temperature = 700–800 °C, time-on-stream: 15 h, at atmospheric pressure	Ethanol conversion: 62%, H_2 yield: ~60%	98
0.3 wt% K–Co|α-Al_2O_3	Incipient wetness impregnation	Continuous flow reactor	GHSV = 60 000 cm^3 g^{-1} h^{-1}, temperature = 500 °C, time-on-stream: 24 h, at atmospheric pressure	Ethanol conversion: 60%, H_2 selectivity: ~94%	93
K–CoZn|α-Al_2O_3	Water/glycerol impregnation	Fixed-bed continuous-flow quartz reactor	Flow rate: 38.5 ml min^{-1}, temperature = 550 °C, under atmospheric pressure, time-on-stream: ~165 h, H_2O/EtOH molar ratio = 4/1	Ethanol conversion: 94%, H_2 selectivity: ~94%	59
Co/SiO_2	Impregnation	Continuous flow micro-reactor	Rate: 2 cm^3 h^{-1}, temperature = 400 °C, EtOH : H_2O molar ratio = 1 : 3	Ethanol conversion: above 90%, H_2 yield: 67%, 9 h stable, 0.02 mg C per g_{cat}·per h	86
1.8% Na–2% Pt/ZrO_2	Incipient wetness impregnation	Fixed bed reactor	GHSV = 381 000 h^{-1}, temperature = 300 °C, P = 1 atm	Ethanol conversion: 51.3%	45
Ni–La_2O_3/ZrO_2	Incipient wetness impregnation	PID reference reactor	W/F ratio = 1.44 g h g^{-1} mol^{-1}, temperature = 550 °C, stability test time = 16 h, H_2O/EtOH molar ratio = 6/1	Ethanol conversion: 81%, H_2 yield: 25%, 2 wt% carbon after 16 h	87
10% Ni–5% La–5% Ce/SBA-15	Modified triblock co-polymer synthesis	Up-flow packed bed reactor	Feeding rate: 3.0 g min^{-1}, temperature = 650 °C	Hydrogen selectivity: 54.3%, no carbon found after 2 h	78
NiMo/SBA-15	Wet impregnation	Isothermal fixed-bed reactor	WHSV = ~156 h^{-1}, temperature = 600 °C, under atmospheric pressure	Ethanol conversion: ~90%, H_2 yield: ~50%, 65 h stable, carbon ~ 5 wt%	79
10 wt% Ni/MM-SBA-15	Glycol assisted impregnation	Two-stage fixed-bed reaction system	GHSV = 6000 h^{-1}, temperature = 600 °C, under atmospheric pressure	H_2 selectivity: 70%, stable for 2 h	80
NiNPs/OH-MBeta	Wetness impregnation	Tubular fixed-bed steel reactor	WHSV = 29.4 h^{-1}, temperature = 350–550 °C, at atmospheric pressure	Ethanol conversion: >85%, H_2 selectivity: 70%, 100 h stable	82
10 wt% Ni/ZIF-8.PEG	Deposition–precipitation	Stainless-steel microreactor	Total volumetric flow rate = 5.6 ml h^{-1}, temperature = 450 °C, at atmospheric pressure, H_2O/C_2H_5OH liquid feed stream with 4 : 1 molar ratio	Ethanol conversion: 88%, H_2 selectivity: 66%, H_2 yield: 52.6%, 50 wt% carbon after 10 h	83
20Ni/ATP	Chemical precipitation	Continuous-flow fixed-bed	WHSV = 12.6 h^{-1}, temperature = 600 °C, P = 1 atm, S/C = 1.5, TOS = 4 h	Ethanol conversion: ~95%, H_2 yield: ~78%, stable for 4 h, carbon 60 mg g_{cat}^{-1}	95

Brief summary

Recent progress on SRE catalysts has provided a comprehensive insight into SRE mechanisms and the role of active metals and supports. To achieve high H_2 yield and high stability in SRE, several key parameters are very important for the catalysts. As the active metals should be cheap and must be active for C–C breaking, Ni and Co are the most common choice. Appropriate doping metals are usually needed to adjust the surface properties to achieve higher H_2 selectivity and stronger coking resistance. The mechanisms include promoting ethanol dehydrogenation, accelerating WGS reaction, and enhancing surface oxygen affinity. Representative outstanding catalysts include $0.2Cu–Ni–Al_2O_3–ZrO_2$,[72] $Ni_{10}–Co/LaFeO_3$,[73] and $Ni_{10}Fe_{10}/MgAl_2O_4$.[75] On the other hand, moderate alkaline supports with high specific area are needed to suppress ethanol dehydration and facilitate carbon elimination, thus significantly reducing coking. Mobile oxygen species also benefit coking gasification. Strong MSI ensures high metal dispersion, which enhances the activity and unfavorable for coking nucleation. It is difficult for one single support to possess all these advantages, so rational doping and the addition of promoters are necessary. CeO_2 is a promising candidate as promoter[78,99,100] or supports.[101–103]

Till now, carbon deposition cannot be absolutely eliminated. Nevertheless, a small amount of filamentous coke is easy to remove by regeneration of spent catalysts, which can be achieved by calcination in air,[68] diluted O_2 (ref. 88) or CO_2.[107] The activity and selectivity of the catalyst can recover in most cases.

Summary and outlook

In recent years, significant progress has been made for SRE catalysts. Non-noble metals (Ni, Co, and Cu-based alloys) on supports with moderate alkalinity and high oxygen storage capacity (CeO_2 based supports) have been proven to be effective. Many catalysts with high H_2 yield and good stability have been reported. However, most of them are still not applicable to the industry. As the SRE process is very complicated, the specific mechanisms of SRE on different catalysts remain controversial. From our point of view, several works are worth focusing on in the future:

(1) SRE is a strong endothermic reaction with high reaction temperature, which leads to high cost and catalyst deactivation. For many similar reactions, such as dry reforming of methane, steam reforming of methanol, steam reforming of glycerol, *etc.*, photothermal catalysis employing clean and infinite solar energy has been introduced as an effective way to reduce reaction temperature.[108–110] Till now, photothermal SRE is rarely reported though Yuan *et al.* have done excellent pioneer work.[111] More further research studies are needed.

(2) Thanks to the fast development of advanced characterization techniques, more in-depth analysis is needed on how different properties of catalysts impact SRE mechanisms, especially the mechanisms of coking. It is very important to further elucidate the role of the relevant properties of active metals, supports, and additives in key carbon deposition reactions, which can guide the design of new highly stable catalysts.

(3) Based on as-known mechanisms, it is necessary to optimize existing catalysts to achieve higher overall performance. On the other hand, exploratory works are also needed to look for promising new materials and new synthesis methods for novel catalysts.

Author contributions

Xiaoqian Feng, Huimin Liu, and Qijian Zhang: writing – review & editing; Yilin Zhao: writing – original draft.

Conflicts of interest

There are no conflicts to declare.

Acknowledgements

This work was supported by the National Natural Science Foundation of China (No. 22202095) and the Nature Science Foundation of Liaoning Province (No. 2022-BS-309).

Notes and references

1 C. Le Quéré, G. P. Peters, P. Friedlingstein, R. M. Andrew, J. G. Canadell, S. J. Davis, R. B. Jackson and M. W. Jones, *Nat. Clim. Change*, 2021, **11**, 197–199.
2 Z. Liu, Z. Deng, G. He, H. Wang, X. Zhang, J. Lin, Y. Qi and X. Liang, *Nat. Rev. Earth Environ.*, 2022, **3**, 141–155.
3 F. Wang, J. D. Harindintwali, Z. Yuan, M. Wang, F. Wang, S. Li, Z. Yin, L. Huang, Y. Fu, L. Li, S. X. Chang, L. Zhang, J. Rinklebe, Z. Yuan, Q. Zhu, L. Xiang, D. C. W. Tsang, L. Xu, X. Jiang, J. Liu, N. Wei, M. Kästner, Y. Zou, Y. S. Ok, J. Shen, D. Peng, W. Zhang, D. Barceló, Y. Zhou, Z. Bai, B. Li, B. Zhang, K. Wei, H. Cao, Z. Tan, L.-b. Zhao, X. He, J. Zheng, N. Bolan, X. Liu, C. Huang, S. Dietmann, M. Luo, N. Sun, J. Gong, Y. Gong, F. Brahushi, T. Zhang, C. Xiao, X. Li, W. Chen, N. Jiao, J. Lehmann, Y.-G. Zhu, H. Jin, A. Schäffer, J. M. Tiedje and J. M. Chen, *The Innovation*, 2021, **2**, 100180.
4 S. Robert, *Green Chem.*, 2021, **23**, 1584.
5 H. B. Aditiya and M. Aziz, *Int. J. Hydrogen Energy*, 2021, **46**, 35027–35056.
6 N. Akhlaghi and G. Najafpour-Darzi, *Int. J. Hydrogen Energy*, 2020, **45**, 22492–22512.
7 S. E. Hosseini and M. A. Wahid, *Renewable Sustainable Energy Rev.*, 2016, **57**, 850–866.
8 A. Sari, E. Sulukan, Z. Dou and T. S. Uyar, *Int. J. Hydrogen Energy*, 2021, **46**, 29680–29693.
9 N. Muradov, *Int. J. Hydrogen Energy*, 2017, **42**, 14058–14088.
10 J. Dufour, D. P. Serrano, J. L. Gálvez, J. Moreno and C. García, *Int. J. Hydrogen Energy*, 2008, **34**, 1370–1376.
11 S. Ramachandran, S. Sabarathinam, S. Manigandan, M. Thangavel, I. Aran, K. Sang-Hyoun, P. Anburajan, G. V. Edwin, B. Kathirvel and P. Arivalagan, *Fuel*, 2021, **291**, 120136.
12 G. Xu, S. Rong, X. Jun and L. Boqiang, *Appl. Energy*, 2021, **285**, 116384.

13 M. K. Moharana, N. R. Peela, S. Khandekar and D. Kunzru, *Renewable Sustainable Energy Rev.*, 2011, **15**, 524–533.
14 R. Moradi and K. M. Groth, *Int. J. Hydrogen Energy*, 2019, **44**, 12254–12269.
15 H. Lee and Y.-K. Park, *Int. J. Hydrogen Energy*, 2020, **45**, 20210–20215.
16 T. Hou, S. Zhang, Y. Chen, D. Wang and W. Cai, *Renewable Sustainable Energy Rev.*, 2015, **44**, 132–148.
17 W. Cai, P. R. d. l. Piscina, K. Gabrowska and N. Homs, *Bioresour. Technol.*, 2013, **128**, 461–471.
18 W.-C. Chiu, R.-F. Horng and H.-M. Chou, *Int. J. Hydrogen Energy*, 2013, **38**, 2760–2769.
19 L. Di, L. Xinyu and G. Jinlong, *Chem. Rev.*, 2016, **116**, 11529–11653.
20 I. Rossetti, A. Tripodi and G. Ramis, *Int. J. Hydrogen Energy*, 2020, **45**, 10292–10303.
21 M. Toor, S. S. Kumar, S. K. Malyan, N. R. Bishnoi, T. Mathimani, K. Rajendran and A. Pugazhendhi, *Chemosphere*, 2020, **242**, 125080.
22 W.-H. Chen, P. P. Biswas, H. C. Ong, T.-B. Nguyen and C.-D. Dong, *Fuel*, 2023, **333**, 126526.
23 J. L. Contreras, J. Salmones, J. A. Colín-Luna, L. Nuño, B. Quintana, I. Córdova, B. Zeifert, C. Tapia and G. A. Fuentes, *Int. J. Hydrogen Energy*, 2014, **39**, 18835–18853.
24 W. Wang and Y. Wang, *Int. J. Hydrogen Energy*, 2008, **33**, 5035–5044.
25 Z. Al-Hamamre and M. A. Hararah, *Int. J. Hydrogen Energy*, 2010, **35**, 5367–5377.
26 M.-N. N. Shafiqah, T. J. Siang, P. S. Kumar, Z. Ahmad, A. Jalil, M. B. Bahari, Q. Van Le, L. Xiao, M. Mofijur and C. Xia, *Environ. Chem. Lett.*, 2022, **20**, 1695–1718.
27 S. Freni, G. Maggio and S. Cavallaro, *J. Power Sources*, 1996, **62**, 67–73.
28 S. Ogo and Y. Sekine, *Fuel Process. Technol.*, 2020, **199**, 106238.
29 Y. Deng, S. Li, L. Appels, H. Zhang, N. Sweygers, J. Baeyens and R. Dewil, *Renewable Sustainable Energy Rev.*, 2023, **175**, 113184.
30 W.-H. Chen, P. P. Biswas, A. T. Ubando, Y.-K. Park, V. Ashokkumar and J.-S. Chang, *Fuel*, 2023, **342**, 127871.
31 G. A. Deluga, J. R. Salge, L. D. Schmidt and X. E. Verykios, *Science*, 2004, **303**, 993–997.
32 R. Baruah, M. Dixit, P. Basarkar, D. Parikh and A. Bhargav, *Renewable Sustainable Energy Rev.*, 2015, **51**, 1345–1353.
33 S. Nanda, R. Rana, Y. Zheng, J. A. Kozinski and A. K. Dalai, *Sustainable Energy Fuels*, 2017, **1**, 1232–1245.
34 E. Y. García and M. A. Laborde, *Int. J. Hydrogen Energy*, 1991, **16**, 307–312.
35 I. Fishtik, A. Alexander, R. Datta and D. Geana, *Int. J. Hydrogen Energy*, 2000, **25**, 31–45.
36 M. Greluk, M. Rotko, G. Słowik and S. Turczyniak-Surdacka, *J. Energy Inst.*, 2019, **92**, 222–238.
37 A. H. Martínez, E. Lopez, L. E. Cadús and F. N. Agüero, *Catal. Today*, 2021, **372**, 59–69.
38 M. Martinelli, C. D. Watson and G. Jacobs, *Int. J. Hydrogen Energy*, 2020, **45**, 18490–18501.
39 M. Greluk, M. Rotko and S. Turczyniak-Surdacka, *Renew. Energy*, 2020, **155**, 378–395.
40 Z. Niazi, A. Irankhah, Y. Wang and H. Arandiyan, *Int. J. Hydrogen Energy*, 2020, **45**, 21512–21522.
41 C. Ruocco, V. Palma and A. Ricca, *Top. Catal.*, 2019, **62**, 467–478.
42 C. A. Chagas, R. L. Manfro and F. S. Toniolo, *Catal. Lett.*, 2020, **150**, 3424–3436.
43 S. Isarapakdeetham, P. Kim-Lohsoontorn, S. Wongsakulphasatch, W. Kiatkittipong, N. Laosiripojana, J. Gong and S. Assabumrungrat, *Int. J. Hydrogen Energy*, 2020, **45**, 1477–1491.
44 A. M. d. Silva, K. R. d. Souza, G. Jacobs, U. M. Graham, B. H. Davis, L. V. Mattos and F. B. Noronha, *Appl. Catal., B*, 2011, **102**, 94–109.
45 M. Martinelli, J. D. Castro, N. Alhraki, M. E. Matamoros, A. J. Kropf, D. C. Cronauer and G. Jacobs, *Appl. Catal., A*, 2021, **610**, 117947.
46 I. Fishtik, A. Alexander, R. Datta and D. Geana, *Int. J. Hydrogen Energy*, 2000, **25**, 31–45.
47 Y. C. Sharma, A. Kumar, R. Prasad and S. N. Upadhyay, *Renewable Sustainable Energy Rev.*, 2017, **74**, 89–103.
48 C. Montero, A. Remiro, B. Valle, L. Oar-Arteta, J. Bilbao and A. G. Gayubo, *Ind. Eng. Chem. Res.*, 2019, **58**, 14736–14751.
49 M. Greluk, W. Gac, M. Rotko, G. Słowik and S. Turczyniak-Surdacka, *J. Catal.*, 2021, **393**, 159–178.
50 A. L. M. da Silva, J. P. den Breejen, L. V. Mattos, J. H. Bitter, K. P. de Jong and F. B. Noronha, *J. Catal.*, 2014, **318**, 67–74.
51 X. Zhao and G. Lu, *Int. J. Hydrogen Energy*, 2016, **41**, 3349–3362.
52 D. K. Liguras, D. I. Kondarides and X. E. Verykios, *Appl. Catal., B*, 2003, **43**, 345–354.
53 M. Bilal and S. D. Jackson, *Catal. Sci. Technol.*, 2013, **3**, 754–766.
54 S. M. de Lima, A. M. Silva, U. M. Graham, G. Jacobs, B. H. Davis, L. V. Mattos and F. B. Noronha, *Appl. Catal., A*, 2009, **352**, 95–113.
55 A. Cifuentes, R. Torres and J. Llorca, *Int. J. Hydrogen Energy*, 2020, **45**, 26265–26273.
56 T. Gu, W. Zhu and B. Yang, *Catal. Sci. Technol.*, 2021, **11**, 7009–7017.
57 P. Ciambelli, V. Palma and A. Ruggiero, *Appl. Catal., B*, 2010, **96**, 190–197.
58 P. Ciambelli, V. Palma and A. Ruggiero, *Appl. Catal., B*, 2010, **96**, 18–27.
59 G. Grzybek, M. Greluk, P. Indyka, K. Góra-Marek, P. Legutko, G. Słowik, S. Turczyniak-Surdacka, M. Rotko, Z. Sojka and A. Kotarba, *Int. J. Hydrogen Energy*, 2020, **45**, 22658–22673.
60 F. Chen, Y. Tao, H. Ling, C. Zhou, Z. Liu, J. Huang and A. Yu, *Fuel*, 2020, **280**, 118612.
61 H. Ma, L. Zeng, H. Tian, D. Li, X. Wang, X. Li and J. Gong, *Appl. Catal., B*, 2016, **181**, 321–331.
62 I. Rossetti, J. Lasso, V. Nichele, M. Signoretto, E. Finocchio, G. Ramis and A. Di Michele, *Appl. Catal., B*, 2014, **150–151**, 257–267.
63 A. Di Michele, A. Dell'Angelo, A. Tripodi, E. Bahadori, F. Sanchez, D. Motta, N. Dimitratos, I. Rossetti and G. Ramis, *Int. J. Hydrogen Energy*, 2019, **44**, 952–964.

64 M. Nuñez Meireles, J. A. Alonso, M. T. Fernández Díaz, L. E. Cadús and F. N. Aguero, *Mater. Today Chem.*, 2020, **15**, 100213.
65 L. Zhao, T. Han, H. Wang, L. Zhang and Y. Liu, *Appl. Catal., B*, 2016, **187**, 19–29.
66 T. S. Moraes, R. C. R. Neto, M. C. Ribeiro, L. V. Mattos, M. Kourtelesis, S. Ladas, X. Verykios and F. Bellot Noronha, *Catal. Today*, 2015, **242**, 35–49.
67 A. Hernández Martínez, E. Lopez, S. Larrégola, O. Furlong, M. S. Nazzarro, L. E. Cadús and F. N. Agüero, *Mater. Today Chem.*, 2022, **26**, 101077.
68 C. H. Campos, G. Pecchi, J. L. G. Fierro and P. Osorio-Vargas, *Mol. Catal.*, 2019, **469**, 87–97.
69 M. C. Sanchez-Sanchez, R. M. Navarro Yerga, D. I. Kondarides, X. E. Verykios and J. L. G. Fierro, *J. Phys. Chem. A*, 2010, **114**, 3873–3882.
70 Ś. Michał and S. Katarzyna, *Int. J. Hydrogen Energy*, 2020, **46**, 555–564.
71 B. Lorenzut, T. Montini, L. De Rogatis, P. Canton, A. Benedetti and P. Fornasiero, *Appl. Catal., B*, 2011, **101**, 397–408.
72 J. Han, J. H. Song, Y. Bang, J. Yoo, S. Park, K. H. Kang and I. K. Song, *Int. J. Hydrogen Energy*, 2016, **41**, 2554–2563.
73 Z. Wang, C. Wang, S. Chen and Y. Liu, *Int. J. Hydrogen Energy*, 2014, **39**, 5644–5652.
74 H. Braga, D. C. de Oliveira, A. R. Taschin, J. B. O. Santos, J. M. R. Gallo and J. M. C. Bueno, *ACS Catal.*, 2021, **11**, 2047–2061.
75 Y. Wu, C. Pei, H. Tian, T. Liu, X. Zhang, S. Chen, Q. Xiao, X. Wang and J. Gong, *JACS Au*, 2021, **1**, 1459–1470.
76 L. Rahmanzadeh and M. Taghizadeh, *Chem. Eng. Technol.*, 2020, **43**, 218–229.
77 F. M. Bkangmo Kontchouo, Y. Shao, S. Zhang, M. Gholizadeh and X. Hu, *Chem. Eng. Sci.*, 2023, **265**, 118257.
78 S. Moogi, I.-G. Lee and J.-Y. Park, *Int. J. Hydrogen Energy*, 2019, **44**, 29537–29546.
79 M. A. Elharati, K.-M. Lee, S. Hwang, A. Mohammed Hussain, Y. Miura, S. Dong, Y. Fukuyama, N. Dale, S. Saunders, T. Kim and S. Ha, *Chem. Eng. J.*, 2022, **441**, 135916.
80 C. M. Parlett, L. J. Durndell, M. A. Isaacs, X. Liu and C. Wu, *Top. Catal.*, 2020, **63**, 403–412.
81 I. C. S. Costa, E. M. Assaf and J. M. Assaf, *Top. Catal.*, 2021, 1–16.
82 S. Wang, B. He, R. Tian, X. Wu, X. An, Y. Liu, J. Su, Z. Yu and X. Xie, *Int. J. Hydrogen Energy*, 2020, **45**, 16409–16420.
83 R. Marjan, F. Shohreh, M. m. Meisam and N. Amideddin, *J. Environ. Chem. Eng.*, 2021, **9**, 105531.
84 T. K. Phung, T. L. M. Pham, A.-N. T. Nguyen, K. B. Vu, H. N. Giang, T.-A. Nguyen, T. C. Huynh and H. D. Pham, *Chem. Eng. Technol.*, 2020, **43**, 672–688.
85 M. Chen, D. Liang, Y. Wang, C. Wang, Z. Tang, C. Li, J. Hu, W. Cheng, Z. Yang, H. Zhang and J. Wang, *Int. J. Hydrogen Energy*, 2021, **46**, 21796–21811.
86 M. S. Batista, R. K. Santos, E. M. Assaf, J. M. Assaf and E. A. Ticianelli, *J. Power Sources*, 2003, **124**, 99–103.
87 C. Pizzolitto, F. Menegazzo, E. Ghedini, G. Innocenti, A. Di Michele, M. Mattarelli, G. Cruciani, F. Cavani and M. Signoretto, *ACS Sustainable Chem. Eng.*, 2020, **8**, 10756–10766.
88 K. Boudadi, A. Bellifa, C. Márquez-Álvarez and V. Cortés Corberán, *Appl. Catal., A*, 2021, **619**, 118141.
89 K. Shi, X. An, Y. Du, Z. Fan, X. Wu and X. Xie, *J. Energy Inst.*, 2022, **104**, 35–45.
90 H. Tian, C. Pei, Y. Wu, S. Chen, Z.-J. Zhao and J. Gong, *Appl. Catal., B*, 2021, **293**, 120178.
91 A. Cao, R. Lu and G. Veser, *Phys. Chem. Chem. Phys.*, 2010, **12**, 13499–13510.
92 H. Meng, Y. Yang, T. Shen, W. Liu, L. Wang, P. Yin, Z. Ren, Y. Niu, B. Zhang, L. Zheng, H. Yan, J. Zhang, F.-S. Xiao, M. Wei and X. Duan, *Nat. Commun.*, 2023, **14**, 3189.
93 G. Grzybek, K. Góra-Marek, P. Patulski, M. Greluk, M. Rotko, G. Słowik and A. Kotarba, *Appl. Catal., A*, 2021, **614**, 118051.
94 S. Yoo, S. Park, J. H. Song and D. H. Kim, *Mol. Catal.*, 2020, **491**, 110980.
95 Y. Wang, C. Wang, M. Chen, Z. Tang, Z. Yang, J. Hu and H. Zhang, *Fuel Process. Technol.*, 2019, **192**, 227–238.
96 Y. Wang, D. Liang, C. Wang, M. Chen, Z. Tang, J. Hu, Z. Yang, H. Zhang, J. Wang and S. Liu, *Renew. Energy*, 2020, **160**, 597–611.
97 G. Zhou, L. Barrio, S. Agnoli, S. D. Senanayake, J. Evans, A. Kubacka, M. Estrella, J. C. Hanson, A. Martínez-Arias, M. Fernández-García and J. A. Rodriguez, *Angew. Chem., Int. Ed.*, 2010, **49**, 9680–9684.
98 S. Roychowdhury, M. M. Ali, S. Dhua, T. Sundararajan and G. R. Rao, *Int. J. Hydrogen Energy*, 2021, **46**, 19254–19269.
99 X. Luo, Y. Hong, H. Zhang, K. Shi, G. Yang and T. Wu, *Int. J. Energy Res.*, 2019, **43**, 3823–3836.
100 M. Wang, S. Y. Kim, Y. Men and E. W. Shin, *Int. J. Hydrogen Energy*, 2022, **47**, 33765–33780.
101 Z. Xiao, Y. Li, F. Hou, C. Wu, L. Pan, J. Zou, L. Wang, X. Zhang, G. Liu and G. Li, *Appl. Catal., B*, 2019, **258**, 117940.
102 Z. Xiao, C. Wu, L. Wang, J. Xu, Q. Zheng, L. Pan, J. Zou, X. Zhang and G. Li, *Appl. Catal., B*, 2021, **286**, 119884.
103 J. Vecchietti, P. Lustemberg, E. L. Fornero, M. Calatayud, S. E. Collins, S. Mohr, M. V. Ganduglia-Pirovano, J. Libuda and A. L. Bonivardi, *Appl. Catal., B*, 2020, **277**, 119103.
104 M. Kourtelesis, T. S. Moraes, L. V. Mattos, D. K. Niakolas, F. B. Noronha and X. Verykios, *Appl. Catal., B*, 2021, **284**, 119757.
105 D. G. Araiza, A. Gómez-Cortés and G. Díaz, *Catal. Today*, 2020, **349**, 235–243.
106 R. Li, C. Liu, L. Li, J. Xu, J. Ma, J. Ni, J. Yan, J. Han, Y. Pan, Y. Liu and L. Lu, *Fuel*, 2023, **336**, 126758.
107 L. Bednarczuk, P. Ramírez de la Piscina and N. Homs, *Int. J. Hydrogen Energy*, 2016, **41**, 19509–19517.
108 W. Zhong, C. Wang, S. Peng, R. Shu, Z. Tian, Y. Du and Y. Chen, *Int. J. Hydrogen Energy*, 2022, **47**, 16507–16517.
109 L. Zhao, M. Tang, F. Wang and X. Qiu, *Fuel*, 2023, **331**, 125748.
110 K. Han, Y. Wang, S. Wang, Q. Liu, Z. Deng and F. Wang, *Chem. Eng. J.*, 2021, **421**, 129989.
111 D. Yuan, Y. Peng, L. Ma, J. Li, J. Zhao, J. Hao, S. Wang, B. Liang, J. Ye and Y. Li, *Green Chem.*, 2022, **24**, 2044–2050.